Monthly Notices
of the
ROYAL ASTRONOMICAL SOCIETY

MNRAS **456,** L11–L15 (2016) doi:10.1093/mnrasl/slv167

Carbon production on accreting neutron stars in a new regime of stable nuclear burning

L. Keek[1]★ and A. Heger[2,3,4]

[1]*Center for Relativistic Astrophysics, School of Physics, Georgia Institute of Technology, 837 State Street, Atlanta, GA 30332-0430, USA*
[2]*Monash Center for Astrophysics, School of Physics and Astronomy, Monash University, Victoria, 3800, Australia*
[3]*Center for Nuclear Astrophysics, Department of Physics and Astronomy, Shanghai Jiao-Tong University, Shanghai 200240, P. R. China*
[4]*School of Physics and Astronomy, University of Minnesota, Minneapolis, MN 55455, USA*

Accepted 2015 October 26. Received 2015 October 8; in original form 2015 July 12

ABSTRACT

Accreting neutron stars exhibit Type I X-ray bursts from both frequent hydrogen/helium flashes as well as rare carbon flashes. The latter (superbursts) ignite in the ashes of the former. Hydrogen/helium bursts, however, are thought to produce insufficient carbon to power superbursts. Stable burning could create the required carbon, but this was predicted to only occur at much larger accretion rates than where superbursts are observed. We present models of a new steady-state regime of stable hydrogen and helium burning that produces pure carbon ashes. Hot CNO burning of hydrogen heats the neutron star envelope and causes helium to burn before the conditions of a helium flash are reached. This takes place when the mass accretion rate is around 10 per cent of the Eddington limit: close to the rate where most superbursts occur. We find that increased heating at the base of the envelope sustains steady-state burning by steepening the temperature profile, which increases the amount of helium that burns before a runaway can ensue.

Key words: accretion, accretion discs – nuclear reactions, nucleosynthesis, abundances – methods: numerical – stars: neutron – X-rays: binaries – X-rays: bursts.

1 INTRODUCTION

In low-mass X-ray binaries hosting a neutron star, hydrogen- and helium-rich material may be transferred from the companion star to the neutron star by Roche lobe overflow. Compression due to a high surface gravity induces nuclear fusion, giving rise to a broad range of observed phenomena. Most prominent are Type I X-ray bursts with typical durations of 10–100 s produced by runaway thermonuclear burning (Grindlay et al. 1976; Woosley & Taam 1976; Maraschi & Cavaliere 1977, see also Lewin, van Paradijs & Taam 1993; Strohmayer & Bildsten 2006). Stable burning is inferred from the absence of bursts at mass accretion rates above ∼10–30 per cent of the Eddington limit (van Paradijs, Penninx & Lewin 1988; Cornelisse et al. 2003). In that case, hydrogen and helium burn continuously in a steady state, without triggering a thermonuclear runaway. All these burning regimes are reproduced by theory (Fujimoto, Hanawa & Miyaji 1981), but there is a large mismatch in the conditions required for certain regimes to occur. For example, bursts are predicted to persist up to ∼100 per cent of the Eddington limit (e.g. Heger, Cumming & Woosley 2007a; Keek, Langer & in 't Zand 2009; Zamfir, Cumming & Niquette 2014).

Many subsequent X-ray bursts or long periods of stable burning of hydrogen and helium burning leave behind an ashes layer that is rich in carbon. Runaway carbon fusion in these ashes is thought to power the rare 'superbursts': hours-long flashes from the same X-ray sources (Cornelisse et al. 2000; Cumming & Bildsten 2001; Strohmayer & Brown 2002). All superbursting neutron stars also exhibit short bursts, but superburst observations constrain the carbon mass fraction to be larger (∼20 per cent; Cumming et al. 2006) than what hydrogen/helium bursts are thought to produce ($\lesssim$5 per cent; e.g. Woosley et al. 2004). Chemical separation could increase the carbon fraction (Medin & Cumming 2011), but would increase the recurrence times. These sources have relatively low burst rates (in 't Zand, Cornelisse & Cumming 2004), suggesting that aside from bursts some stable burning occurs. This may produce larger amounts of carbon (e.g. Stevens et al. 2014), but no such stable burning mode was predicted by theory.

In this Letter, we investigate the ignition conditions of hydrogen and helium burning, and we identify a new stable burning regime at mass accretion rates bordering the burst regimes. Furthermore, time-dependent multizone models show that this regime is more

★ E-mail: l.keek@gatech.edu

© 2015 The Authors
Published by Oxford University Press on behalf of the Royal Astronomical Society

Downloaded from http://mnrasl.oxfordjournals.org/ at ULB Bonn, Abt. MNL on April 13, 2016

prevalent when the base heating of the neutron star envelope is strong.

2 NUMERICAL METHODS

2.1 One-zone model

We construct a simple one-zone numerical model to study the ignition conditions of hydrogen and helium burning as well as the stability of the burning processes in the neutron star envelope. The zone is given a temperature, T, and density, ρ, as well as mass fractions X, Y, Z, for ^{1}H, ^{4}He, and the combined CNO isotopes, respectively. We use a solar accretion composition of $X = 0.73$, $Y = 0.25$, and $Z = 0.02$, and we assume all accreted CNO is initially ^{14}N. The Helmholtz equation of state and opacity routines (Timmes 2000; Timmes & Swesty 2000) are employed to calculate the pressure, P, and opacity, κ. The column depth is derived as $y = P/g$. We use a local gravitational acceleration $g = 1.86 \times 10^{14}\,\mathrm{cm\,s^{-2}}$, corresponding to a neutron star with a gravitational mass of $1.4\,M_\odot$ and a radius of 10 km in the Newtonian case or 11.2 km for General Relativity (e.g. Keek & Heger 2011).

Radiative cooling is implemented with a specific rate of (e.g. Fujimoto et al. 1981)

$$\epsilon_{\mathrm{cool}} = \frac{acT^4}{3\kappa y^2}. \quad (1)$$

We calculate the specific energy generation rate from nuclear burning, ϵ_{nuc}. For helium burning, we use the 3α rate from Fynbo et al. (2005). For hydrogen burning, we employ the hot β-limited CNO cycle (βCNO) for temperatures $T > 0.8 \times 10^8$ K following Bildsten (1998), and at lower temperatures, the CNO cycle using the ^{14}N(p, γ)^{15}O rate as the slowest part of the cycle following Kippenhahn & Weigert (1994). Screening is implemented following Graboske et al. (1973). Finally, the base of the envelope is heated by pycnonuclear and electron-capture reactions in the neutron star crust (Haensel & Zdunik 1990, 2003; Gupta et al. 2007; Schatz et al. 2014), or possibly by the dissipation of rotational energy at the bottom of the ocean (Inogamov & Sunyaev 2010). The amount of heat generated per accreted nucleon, Q_{b}, is treated as a free parameter, and we include base heating as a specific rate: $\epsilon_{\mathrm{b}} = Q_{\mathrm{b}}\dot{m}/y$, where $\dot{m}$ is the specific mass accretion rate. We use a typical value for Q_{b} of $0.1\,\mathrm{MeV\,u^{-1}}$ (e.g. Cumming et al. 2006). The total heating rate is $\epsilon_{\mathrm{heat}} = \epsilon_{\mathrm{nuc}} + \epsilon_{\mathrm{b}}$. We assume the (small) contribution from compressional heating to be part of Q_{b} (e.g. Fujimoto et al. 1981).

In the steady-state case, we determine $\dot{m}$ by equating the timescales for burning and accretion, $\tau_{\mathrm{nuc}} = \tau_{\mathrm{acc}}$, with $\tau_{\mathrm{acc}} \equiv y/\dot{m}$:

$$\dot{m} = y/\tau_{\mathrm{nuc}}. \quad (2)$$

For helium burning, $\tau_{\mathrm{nuc}} \equiv E_{\mathrm{nuc}}Y/\epsilon_{\mathrm{nuc}}$, where $E_{\mathrm{nuc}} = 6.97 \times 10^{18}\,\mathrm{erg\,g^{-1}}$ is the 3α energy yield per unit mass; for hydrogen burning through the βCNO cycle, τ_{nuc} is set by the sum of the half lives of ^{14}O and ^{15}O, $\tau_\beta = 192.86$ s: $\tau_{\mathrm{nuc}} \equiv \frac{14X}{4Z}\tau_\beta$, where 14 accounts for the mass number of ^{14}N, and 4 is the net number of protons that are burned in each cycle. We express $\dot{m}$ as a fraction of the Eddington limited value for solar composition: $\dot{m}_{\mathrm{Edd}} = 8.78 \times 10^4\,\mathrm{g\,s^{-1}}$.

2.2 Multizone time-dependent models

We employ the one-dimensional multizone hydrodynamics code KEPLER (Weaver, Zimmerman & Woosley 1978) to create time-dependent models of the neutron star envelope. The version of KEPLER and the setup of the models is similar to a previous study by Keek, Cyburt & Heger (2014) (see also Woosley et al. 2004; Heger et al. 2007a,b). We refer to these studies for details of the code, and here we summarize the main characteristics of our models. The code includes a large nuclear network using thermonuclear reaction rates from the REACLIB 2.0 compilation (Cyburt et al. 2010). The network includes all CNO and βCNO cycle reactions, the 3α process using the rate from Caughlan & Fowler (1988),[1] as well as many other reactions such as break-out from the βCNO cycle. We resolve the neutron star envelope in the radial direction. Material of solar composition is accreted on to a 2×10^{25} g iron substrate, which acts as a thermal buffer into which heat from nuclear burning can dissipate. Crustal heating is implemented as an inflowing heat flux at the inner zone. The same accretion composition and neutron star parameters are used as for the one-zone model (Section 2.1). The results in this Letter are presented without GR corrections or redshifts (see Keek & Heger 2011).

3 RESULTS

3.1 Ignition conditions

We use the one-zone model to reproduce the ignition conditions of hydrogen and helium burning derived by Fujimoto et al. (1981). Steady-state burning requires a balance between heating and cooling: $\epsilon_{\mathrm{heat}} = \epsilon_{\mathrm{cool}}$. For a range of temperatures, we determine the column depth where this condition is met for hydrogen and helium burning separately ('stable' in Fig. 1), and during stable burning the respective element is depleted at that location. A thermonuclear runaway ensues when the heating rate increases faster with T than the cooling rate. Both for hydrogen and helium burning we locate the boundary of the unstable region ('unstable' in Fig. 1):

$$\frac{\mathrm{d}\epsilon_{\mathrm{heat}}}{\mathrm{d}T} = \frac{\mathrm{d}\epsilon_{\mathrm{cool}}}{\mathrm{d}T}. \quad (3)$$

Material accreted on to a neutron star is compressed and heated over time, such that it moves to higher y and T in Fig. 1. The burning behaviour is determined by where the 'stable' and 'unstable' lines are reached (Fujimoto et al. 1981; Fushiki & Lamb 1987; Bildsten 1998). Although CNO burning of hydrogen is unstable at low temperatures, over most of the considered temperature range hydrogen burning is stable, because the βCNO rate is independent of temperature. The stability of helium burning changes at $T \simeq 5 \times 10^8$ K (we take the location to be where $\mathrm{d}T/\mathrm{d}y = 0$; e.g. Zamfir et al. 2014). Furthermore, as the stable hydrogen line crosses the unstable helium line, helium flashes may occur either before hydrogen is depleted or after all hydrogen has been burned to helium. Two helium ignition curves are, therefore, presented: one for the accreted helium fraction $Y = 0.25$ and one where all hydrogen has burned to produce $Y = 0.98$. The transition between pure-helium bursts and mixed hydrogen/helium bursts is at $T \simeq 2 \times 10^8$ K.

3.2 Helium depletion before runaway

These ignition conditions are calculated assuming that hydrogen and helium burning are independent. If only helium is accreted, the temperature increases with depth until ignition is reached. Because of the strong temperature dependence of the 3α rate, very little helium burns before the ignition depth. If, however, hydrogen burning

[1] Within the temperature range considered in our study, the Caughlan & Fowler (1988) and Fynbo et al. (2005) 3α rates differ at most 4 per cent.

Downloaded from http://mnrasl.oxfordjournals.org/ at ULB Bonn, Abt. MNL on April 13, 2016

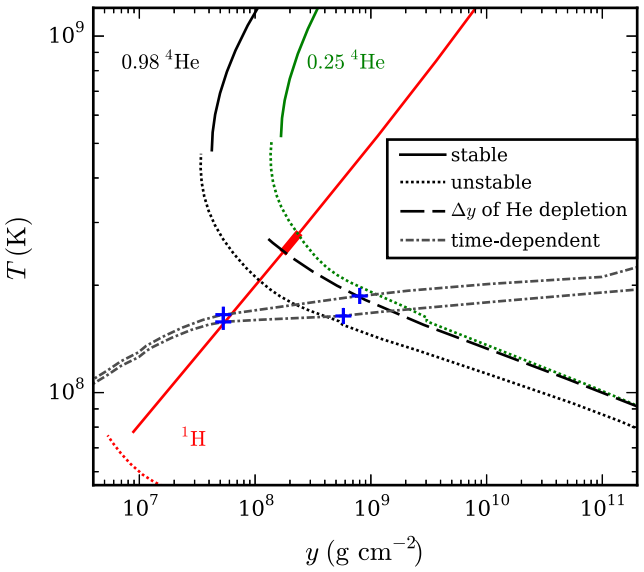

Figure 1. Column depth, y, as a function of temperature, T, for stable and unstable burning of H and He from a solar accretion composition, as well as a He mass fraction of 0.98 when all H has burned to He. Accreted material moves to larger y and T with time, and thus reaches any of the ignition curves. Starting at the stable H line, stable burning depletes He after Δy: the He depletion depth is the stable H line *plus* Δy. The thick solid line indicates where the new stable burning regime of H and He occurs when $\Delta y <$stable H line. The temperature profiles for two time-dependent models are shown: steady-state burning (upper line; $Q_{\rm b} = 0.75\,{\rm MeV\,u^{-1}}$) and just prior to unstable He ignition (lower; $Q_{\rm b} = 0.1\,{\rm MeV\,u^{-1}}$). Their respective locations of H and He depletion are marked with '+'.

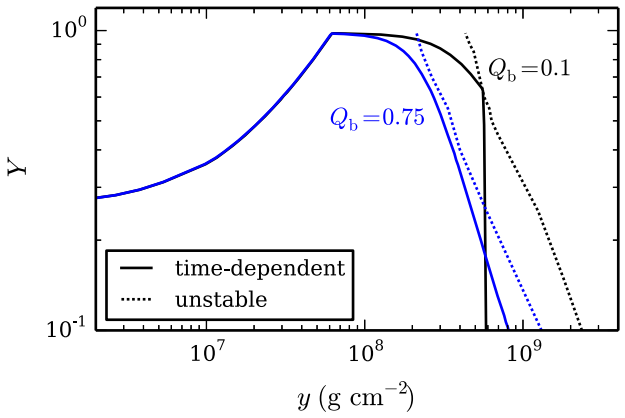

Figure 2. Helium mass fraction, Y, as a function of column depth, y, for two time-dependent models with base heating, $Q_{\rm b}$, in units of MeV u^{-1}. They overlap at $y < 6 \times 10^7$ g cm^{-2}, but at larger depth Y drops faster for the hotter model. Dotted lines mark the conditions for unstable ignition for the two models. The colder model hits the unstable curve and ignites a burst, whereas the hotter model does not reach its unstable curve and has stable burning.

takes place at shallow depths, the envelope is heated substantially, and helium burning is initiated already before its ignition curve is reached. Therefore, before helium burning dominates the energy generation rate, some helium already burns away.

For each point on the stable hydrogen burning line (Fig. 1), we calculate the 3α burning rate assuming all hydrogen has been converted to helium, and we determine the helium burning timescale, $\tau_{\rm nuc}$ (Section 2.1). Given the $\dot{m}$ associated with steady-state hydrogen burning (equation 2), we estimate the change in column during $\tau_{\rm nuc}$ as $\Delta y = \tau_{\rm nuc}\dot{m}$. Here, we assume that the temperature remains constant going to larger values of y (e.g. Fujimoto et al. 1981), and we neglect the small increase in $\epsilon_{\rm nuc}$ from the increasing density. Where Δy is smaller than the depth of stable ^{1}H burning (Fig. 1), helium is depleted at a depth close to where hydrogen burns: both hydrogen and helium burning proceed in a steady-state, and no thermonuclear runaway occurs. This is a new regime of stable nuclear burning. It happens only in a small temperature interval around $T = 2.6 \times 10^8$ K, which is associated with a small range of accretion rates $0.08 < \dot{m}/\dot{m}_{\rm Edd} < 0.11$ (thick solid line in Fig. 1). At lower T pure helium bursts ignite, whereas at higher T mixed hydrogen/helium bursts occur.

This is a simplistic approximation of time-dependent burning. Although it gives a good qualitative description of the behaviour, time-dependent models are required for accurate quantitative predictions as well as for a better understanding of the new stable burning regime.

3.3 Two time-dependent simulations

For $\dot{m} = 0.1\,\dot{m}_{\rm Edd}$ and $Q_{\rm b} = 0.1\,{\rm MeV\,u^{-1}}$, where the one-zone model predicts the new stable regime, a KEPLER model exhibits mixed H/He bursts, indicating the new regime must occur at somewhat lower $\dot{m}$ for multizone models. Therefore, we create two KEPLER simulations with $\dot{m} = 0.02\,\dot{m}_{\rm Edd}$: one with the same $Q_{\rm b} = 0.1\,{\rm MeV\,u^{-1}}$ as the one-zone models, and one with stronger base heating of $Q_{\rm b} = 0.75\,{\rm MeV\,u^{-1}}$. As expected from Fig. 1, the first model exhibits pure helium bursts after hydrogen is depleted (similar to model Zm by Woosley et al. 2004). The second model, however, displays the new steady-state regime, even though $\dot{m}$ is much lower than where we expected it to occur. We compare the ignition conditions – which exhibit for $Q_{\rm b} = 0.75\,{\rm MeV\,u^{-1}}$ only small shifts with respect to $Q_{\rm b} = 0.1\,{\rm MeV\,u^{-1}}$ – to the T-profiles of the two models, where for the unstable model we select a time just prior to the runaway (Fig. 1). The locations where, respectively, the hydrogen and helium mass fractions are reduced by an order of magnitude agree well with the one-zone estimates.

Even though the two models have roughly similar temperature profiles, their burning behaviour is rather different. Up to the depth of hydrogen-depletion, the helium mass fraction is identical for both models (Fig. 2). For the steady-state model, the temperature profile is slightly steeper (Fig. 1), and the strong temperature dependence of the 3α reaction causes helium to burn faster than in the other model. As Y drops, the relevant unstable ignition curve moves to larger y. We create a series of ignition curves for a range of Y, and show their points of intersection with the T-profiles of the KEPLER models (Fig. 2). For the unstable model, Y is reduced by stable burning to 0.63 before it hits the instability line and ignites a burst (Fig. 2; see also Woosley et al. 2004). For the steady-state model, however, stable helium burning proceeds fast enough to avoid its instability line, and a thermonuclear runaway is never reached.

We study the steady-state model in more detail. 1.9 yr of accretion and burning were simulated, during which time the burning layer was replenished 124 times. The helium mass fraction peaks at the depth where hydrogen is depleted, and rapidly decreases with increasing depth before the conditions for runaway 3α burning are reached (Fig. 3). The temperature in the helium burning region is below $T = 2 \times 10^8$ K, which means that the $^{12}{\rm C}(\alpha,\gamma)^{16}{\rm O}$ reaction is very slow compared to 3α, and α-capture is inefficient. Moreover, because almost all ^{12}C is produced at depths where hydrogen is depleted, $^{12}{\rm C}(p,\gamma)^{13}{\rm N}$ does not play a role either. The burning

Downloaded from http://mnrasl.oxfordjournals.org/ at ULB Bonn, Abt. MNL on April 13, 2016

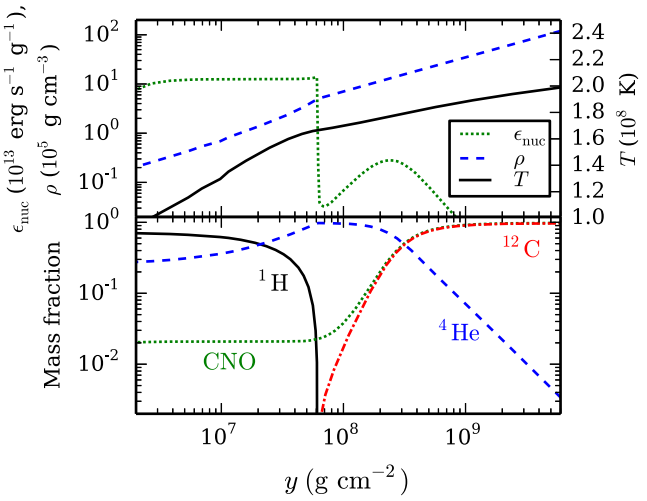

Figure 3. Structure of the neutron star envelope as a function of column depth, y, from a time-dependent multizone simulation of steady-state burning. Top: specific energy generation rate, $\epsilon_{\rm nuc}$, density, ρ, and temperature, T. Bottom: mass fractions for several isotopes. CNO is the sum for all C, N, and O isotopes including ^{12}C. At $y \lesssim 4 \times 10^7$ g cm^{-2} CNO consists mainly of ^{14}O and ^{15}O.

ashes, therefore, consist exclusively of 98 per cent ^{12}C in addition to the 2 per cent accreted CNO mass fraction. The latter are predominantly ^{14}N and ^{15}N from the βCNO cycle with a ratio of about 1 : 2.

4 DISCUSSION

We have identified a new steady-state nuclear burning regime on accreting neutron stars. A range of burning behaviour takes place as a function of $\dot{m}$, and the new regime occurs in a small $\dot{m}$ interval close to 0.1 $\dot{m}_{\rm Edd}$ between the pure helium bursts and the mixed hydrogen/helium bursts. We summarize the different burning regimes in Table 1, although it should be understood that the boundaries between regimes can be modified by, e.g. the metallicity (Woosley et al. 2004), the details of CNO break-out (Fisker et al. 2007; Keek et al. 2014), rotational mixing (Piro & Bildsten 2007; Keek et al. 2009), and base heating (Keek et al. 2009; Zamfir et al. 2014). The small size of the $\dot{m}$ interval may explain why it has not been identified in observations. The mechanism that we describe to burn all helium stably occurs to a lesser extent in the regime of pure helium flashes, where part of the helium is burned before the thermonuclear runaway (Woosley et al. 2004). For accretion rates approaching the new stable regime, this part may be larger.

Table 1. Theoretical nuclear burning regimes [a].

$\dot{m}/\dot{m}_{\rm Edd}$	Burning regime
	Deep H flash (burns He)
∼0.1 per cent [b]	
	Shallow H flashes and deep He flash
0.4 per cent	
	He flash (stable H burning)
8 per cent	
	Stable H/He burning
11 per cent	
	Mixed H/He flash
∼100 per cent [c]	Marginally stable burning of H/He
	Stable H/He burning

Notes. [a]For solar accretion composition and $Q_{\rm b} = 0.1$ MeV u^{-1}.
[b]Peng, Brown & Truran (2007), including sedimentation.
[c]Heger et al. (2007a). See also Keek et al. (2009), Zamfir et al. (2014), Keek et al. (2014).

In time-dependent multizone models, we find that the same steady-state regime can take place at lower $\dot{m}$, if the base heating is stronger. We used $Q_{\rm b} = 0.75$ MeV u^{-1}, which is in line with the amount of heat generated by electron captures in the crust (Gupta et al. 2007). At lower $\dot{m}$, a higher value of $Q_{\rm b}$ is actually expected, because of the temperature sensitivity of neutrino cooling (e.g. Cumming et al. 2006). Furthermore, strong base heating may be needed to explain the observed recurrence times of superbursts (Keek & Heger 2011) and the ignition of superbursts in transients (Keek et al. 2008; Altamirano et al. 2012). The temperature in the outer envelope is largely set by βCNO burning, whereas at the bottom of the envelope crustal heating sets an inflowing flux, such that a higher $Q_{\rm b}$ leads to a higher temperature at the inner boundary. The temperature profile is, therefore, steeper for the model with a higher $Q_{\rm b}$. The boundary of the new steady-state regime is thus strongly dependent on $Q_{\rm b}$, and a large series of time-dependent or steady-state models are required to investigate it.

4.1 Superburst fuel

Assuming all energy is provided by carbon burning, cooling models infer from superburst light curves a carbon mass fraction of 15–26 per cent (Cumming et al. 2006). Part of the energetics could originate from photodisintegration of heavy isotopes near the *rp*-process end-point (Schatz, Bildsten & Cumming 2003), but the composition of the ashes is likely dominated by iron-group nuclei (Woosley et al. 2004). Unstable burning produces at most 5 per cent ^{12}C (e.g. Woosley et al. 2004), whereas the new steady-state regime yields as much as 98 per cent: neither gives the amount inferred for superbursts. Superbursting sources have relatively high values of the ratio of the fluence in-between and during bursts (the so-called α-parameter; in 't Zand et al. 2004), which suggests that part of the accreted hydrogen and helium burns in a stable manner and part in bursts. To obtain 20 per cent ^{12}C, the steady-state mode must be active 16 per cent of the time. As the steady-state occurs in a small $\dot{m}$ range, the 16 per cent duty cycle may be provided by the intrinsic variations in $\dot{m}$. Alternatively, there could be a hybrid between the bursting and stable modes, where a substantial part of ^{4}He burns stably as in the steady-state regime, but an instability is triggered on a delayed time-scale. This regime would be different from the 'delayed mixed bursts' proposed by Narayan & Heyl (2003). Further time-dependent simulations are needed to study the transition between the different regimes, and attention must be given to the possibility of some carbon destruction prior to superburst ignition (e.g. Keek, Heger & in't Zand 2012).

5 CONCLUSIONS

We present models of a new steady-state nuclear-burning regime for hydrogen and helium mixtures accreted on to neutron stars. As hydrogen burns stably via the hot CNO cycle, the increased temperature induces 3α burning of helium. This mechanism fully depletes helium in steady-state at mass accretion rates of ∼10 per cent of the Eddington limit, bordered by burst regimes at lower and higher accretion rates. Enhanced base heating can steepen the temperature profile and sustain the steady-state regime, extending the range of accretion rates where stable burning is active. Pure-carbon ashes are

Downloaded from http://mnrasl.oxfordjournals.org/ at ULB Bonn, Abt. MNL on April 13, 2016

produced, which may power the rare energetic superbursts. In fact, more carbon is produced than needed to explain the fuel mixture of superbursts. Steady-state burning only needs to occur ∼16 per cent of the time. The new stable burning mode could contribute to the large values of the α-parameter observed for superbursting sources.

In future papers, we will perform simulations to investigate the dependence of this burning mode on base heating, metallicity, and other parameters. Large burst catalogues such as MINBAR (Keek et al. 2010) will be employed to constrain the observational signature.

ACKNOWLEDGEMENTS

The authors thank F. X. Timmes for public availability of the Helmholtz EOS and opacity routines at http://cococubed.asu.edu, and they are grateful for discussions with A. Cumming and E. F. Brown. LK acknowledges support from NASA ADAP grant NNX13AI47G. AH is supported by an ARC Future Fellowship (FT120100363). This material is based upon work supported by the National Science Foundation under Grant No. PHY-1430152 (JINA Center for the Evolution of the Elements).

REFERENCES

Altamirano D. et al., 2012, MNRAS, 426, 927
Bildsten L., 1998, in Buccheri R., van Paradijs J., Alpar A., eds, The Many Faces of Neutron Stars. Dordrecht, Kluwer, p. 419
Caughlan G. R., Fowler W. A., 1988, At. Data Nucl. Data Tables, 40, 283
Cornelisse R., Heise J., Kuulkers E., Verbunt F., in't Zand J. J. M., 2000, A&A, 357, L21
Cornelisse R. et al., 2003, A&A, 405, 1033
Cumming A., Bildsten L., 2001, ApJ, 559, L127
Cumming A., Macbeth J., in 't Zand J. J. M., Page D., 2006, ApJ, 646, 429
Cyburt R. H. et al., 2010, ApJS, 189, 240
Fisker J. L., Tan W., Görres J., Wiescher M., Cooper R. L., 2007, ApJ, 665, 637
Fujimoto M. Y., Hanawa T., Miyaji S., 1981, ApJ, 247, 267
Fushiki I., Lamb D. Q., 1987, ApJ, 323, L55
U.Fynbo H. O. et al., 2005, Nature, 433, 136
Graboske H. C., Dewitt H. E., Grossman A. S., Cooper M. S., 1973, ApJ, 181, 457
Grindlay J., Gursky H., Schnopper H., Parsignault D. R., Heise J., Brinkman A. C., Schrijver J., 1976, ApJ, 205, L127
Gupta S., Brown E. F., Schatz H., Möller P., Kratz K.-L., 2007, ApJ, 662, 1188
Haensel P., Zdunik J. L., 1990, A&A, 227, 431
Haensel P., Zdunik J. L., 2003, A&A, 404, L33
Heger A., Cumming A., Woosley S. E., 2007a, ApJ, 665, 1311
Heger A., Cumming A., Galloway D. K., Woosley S. E., 2007b, ApJ, 671, L141
in 't Zand J. J. M., Cornelisse R., Cumming A., 2004, A&A, 426, 257
Inogamov N. A., Sunyaev R. A., 2010, Astron. Lett., 36, 848
Keek L., Heger A., 2011, ApJ, 743, 189
Keek L., in 't Zand J. J. M., Kuulkers E., Cumming A., Brown E. F., Suzuki M., 2008, A&A, 479, 177
Keek L., Langer N., in 't Zand J. J. M., 2009, A&A, 502, 871
Keek L., Galloway D. K., in 't Zand J. J. M., Heger A., 2010, ApJ, 718, 292
Keek L., Heger A., in't Zand J. J. M., 2012, ApJ, 752, 150
Keek L., Cyburt R. H., Heger A., 2014, ApJ, 787, 101
Kippenhahn R., Weigert A., 1994, Stellar Structure and Evolution. Springer-Verlag, Berlin
Lewin W. H. G., van Paradijs J., Taam R. E., 1993, Space Sci. Rev., 62, 223
Maraschi L., Cavaliere A., 1977, in Müller E. A., ed., Highlights in Astronomy, Vol. 4. Reidel, Dordrecht, p. 127
Medin Z., Cumming A., 2011, ApJ, 730, 97
Narayan R., Heyl J. S., 2003, ApJ, 599, 419
Peng F., Brown E. F., Truran J. W., 2007, ApJ, 654, 1022
Piro A. L., Bildsten L., 2007, ApJ, 663, 1252
Schatz H., Bildsten L., Cumming A., 2003, ApJ, 583, L87
Schatz H. et al., 2014, Nature, 505, 62
Stevens J., Brown E. F., Cumming A., Cyburt R., Schatz H., 2014, ApJ, 791, 106
Strohmayer T., Bildsten L., 2006, Lewin W., van der Klis M., eds, Compact Stellar X-ray Sources. Cambridge Univ. Press, Cambridge, p. 113
Strohmayer T. E., Brown E. F., 2002, ApJ, 566, 1045
Timmes F. X., 2000, ApJ, 528, 913
Timmes F. X., Swesty F. D., 2000, ApJS, 126, 501
van Paradijs J., Penninx W., Lewin W. H. G., 1988, MNRAS, 233, 437
Weaver T. A., Zimmerman G. B., Woosley S. E., 1978, ApJ, 225, 1021
Woosley S. E., Taam R. E., 1976, Nature, 263, 101
Woosley S. E. et al., 2004, ApJS, 151, 75
Zamfir M., Cumming A., Niquette C., 2014, MNRAS, 445, 3278

This paper has been typeset from a TEX/LATEX file prepared by the author.

Downloaded from http://mnrasl.oxfordjournals.org/ at ULB Bonn, Abt. MNL on April 13, 2016